Korean J. Chem. Eng., **27**(6), 1901-1905 (2010)
DOI: 10.1007/s11814-010-0289-1

Preparation of high purity nano silica particles from blast-furnace slag

Sun-Jae Kim*, Seong-Gyu Seo, and Sang-Chul Jung***,†**

*Department of Nano Science and Technology, Sejong University, Seoul 143-747, Korea
**Department of Civil & Environmental Engineering, Chonnam National University, Jeonnam 550-749, Korea
***Department of Environmental Engineering, Sunchon National University, Jeonnam 540-742, Korea
(*Received 20 January 2010 • accepted 7 March 2010*)

Abstract−High purity nano silica was synthesized using acid treatment and surface modification from blast-furnace slag generated in the steel industry. Blast-furnace slag was treated with nitric acid to extract high-purity insoluble silica. Nano silica was then produced using filtration and surface modified by cation surfactant- Cetyltrimethyl Ammonium Bromide (CTAB). The Zeta potential of silica was tested under various alkaline conditions. Synthesized silica remained electronegative throughout the pH range tested and the number of hydroxyl groups existing on the silica surface was highest when the pH was 9. The size of silica particles was smallest when the modification temperature was 60 °C. The average size of silica particles modified with 3 wt% CTAB was 107.89 nm, while the average size of unmodified silica was 240.38 nm. After extracting silica, pH of the remaining solution was adjusted by adding CaO and then high-purity calcium nitrate crystals were extracted using solubility difference. It was found experimentally that enriching the solution to a high specific gravity (1.63-1.65) before crystallization is preferable for efficient calcium nitrate recovery.

Key words: Nano Silica, Slag, Surface Modification, Zeta Potential, Particle Size

INTRODUCTION

In the steel industry consisting of complex processes including iron making, steel making, and rolling, a number of different kinds of by-products and wastes are produced resulting from the consumption of large amounts of raw materials and energy [1,2]. Production of these by-products and wastes amounts to 65% of that of the main product, steel [3]. Slag accounts for about 80% of solid state by-products and wastes, whereas the remainder is composed of dust and sludge. Generally, slag produced in steel mills is divided into blast-furnace slag (referred to as "blast slag" hereafter) produced in the blast furnace process and steel-making slag produced in the steel making process [4]. In the blast furnace process, iron ore, coke, and limestone are melted at about 1,500 °C where melted slag, composed of non-iron mineral components, is formed. Melted slag is separated from melted iron by using density difference and then cooled into solid state. Cooled slag is divided into palletized slag (air-cooled) and granulated slag (water-cooled) based on the cooling method. The main components of slag are CaO and SiO_2. Slag can be used as raw material for making cement and concrete based on its particle morphology and characteristics [5]. The value-added of application of slag, however, remains very low. One of the fundamental reasons for the difficulties and problems of slag application is that slag has been used through simple and passive ways of treatments that produce low-value-added products. For example, most blast slag is used as raw material for cement manufacture through a very simple physical process without any special treatment that can create value added [6,7].

In this study, SiO_2 and CaO, which are the main components of slag, were extracted from slag to be used as high-value-added material. Slag was treated with nitric acid to extract SiO_2. Nano silica was produced by using filtration and surface modification of this SiO_2. Nano silica can be used as high-value-added material for construction and medical service [8-10]. After extracting SiO_2, pH of the remaining solution was adjusted by adding CaO and then high-purity calcium nitrate crystals were extracted using solubility difference. Calcium nitrate is used in agriculture and other industries with increasing demand.

EXPERIMENTAL

The slag used in this study was granulated blast slag of P steel mill that had been piled up separately. After a grinding process, only grains with particle size of 50-140 mesh (0.3-0.1 mm) were sieved out and used for experiments.

Table 1 shows the chemical composition of the blast slag used in this study. Slag is a complex compound composed of different oxides as shown in Table 1. Excess nitric acid (Daejung Chem. LTD, 60-62%) was used to elute metal components as expressed in Eq. (1). Silica, which is not soluble in acid, was filtrated out and converted into nano silica by using surface modification.

$$\text{Slag}+HNO_3(\text{excess})\rightarrow Ca(NO_3)_2+SiO_2\downarrow+M(NO_3)n \quad (1)$$

where, M is Al, Mg, Fe, Ti, etc.

Filtered solution contains calcium nitrate and metal nitrates ($M(NO_3)_n$ with M=Al, Mg, Fe, Ti, etc.) mixed with excess nitric acid.

Table 1. Chemical composition of the blast slag used in this study

Composition	SiO_2	CaO	Al_2O_3	Fe	MgO	MnO	S	TiO_2
Wt%	33.5	41.8	13.6	0.4	6.4	0.5	1.0	1.3

†To whom correspondence should be addressed.
E-mail: jsc@sunchon.ac.kr

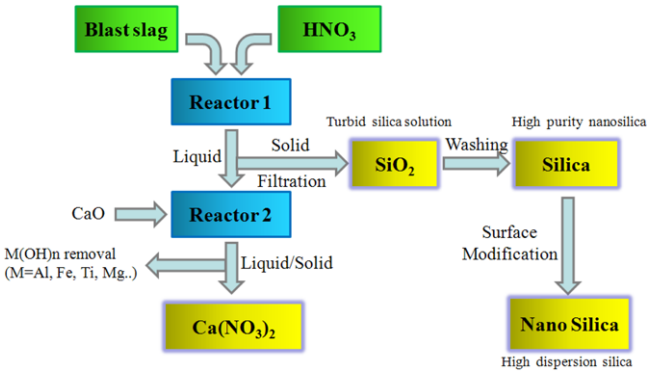

Fig. 1. Flow diagram for synthesis of nano silica particles and calcium nitrate from blast slag.

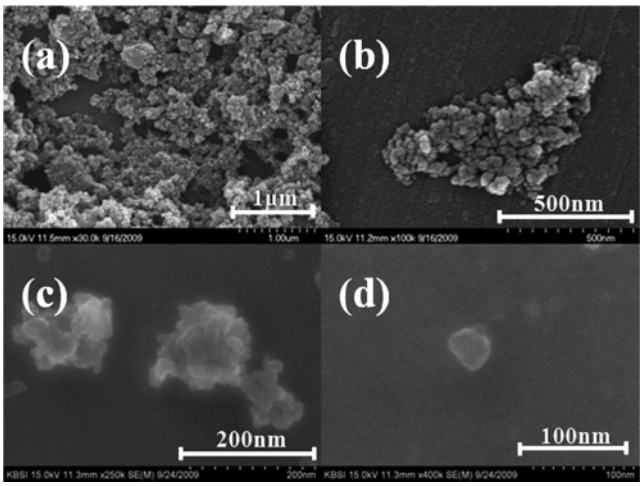

Fig. 2. FE-SEM micrograph images of silica aggregates ((a) and (b)) and modified silica nanoparticles by 3 wt% CTAB at 60 °C ((c) and (d)).

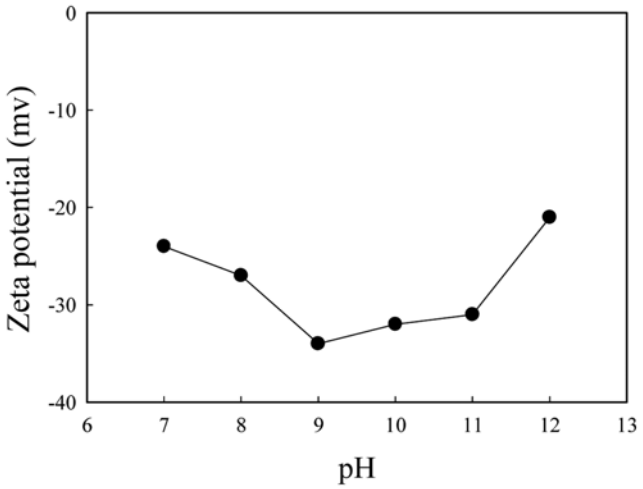

Fig. 3. Zeta potential of the silica particles at different pH conditions.

Therefore, by adding CaO (Yakuri pure Chem. LTD, 98%) that increased pH of the solution, $M(NO_3)_n$ components could be converted into hydroxides, which precipitated due to their low solubility products leaving high-purity calcium nitrate solution. Fig. 1 shows the flow diagram for synthesis of nano silica particles and calcium nitrate used in this study.

The volume of the reactor for the slag-nitric acid reaction was 2 L. The amount of slag-to-nitric acid was 1 : 4. Reaction time was 1 hour and precipitated silica was filtrated by using paper filters (Hyundai Co., 1 μm) High viscosity of the solution after the slag-nitric acid reaction makes the filtration of silica difficult. Therefore, the same amount of distilled water as that of nitric acid used was added before filtrating out silica. Silica obtained in this way was washed five times with distilled water in an ultrasonic cleaner and then was dried in an oven set at 200 °C. The purity of the products, silica and calcium nitrate, was measured using ICP/MS (Perkin Elmer DRC-II). Silica particles were characterized by field emission microscopy (Hitachi, S-4800), zeta potential meter (Photal Co., ELS-8000), particle size analyzer (Photal Co., ELS-8000), FT-IR (Thermo Co., Nicolet 380), and TGA (Scinco Co., STA-1500).

RESULTS AND DISCUSSION

1. Characteristics of Extracted Silica Particles

The chemical composition of silica particles obtained in this study was analyzed by using ICP/MS. Table 2 shows the result. The purity of silica was very high (98.87%). In particular, boron and phosphorus, which significantly degrade silica as a raw material for metal silicon manufacture, were not detected. Therefore, the silica obtained in this study can be used as a basic raw material for solar battery.

The extracted silica particles were observed with FE-SEM and the results are shown in Fig. 2(a) and 2(b). Observed were aggregates of primary silica particles with diameters of about 30-50 nm. The average size of silica aggregates was 240.38 nm (Fig. 2(b)). This result indicates that silica nanoparticles can be obtained if the primary particles are separated by using surface modification.

To graft the more alkyl groups on the silica nano-particles surface, the Zeta potential characteristics of silica particles should be tested before the surface modification process. In the preliminary experiment, alkaline condition was shown to be appropriate for the surface modification process. Therefore, the zeta potential of silica samples was tested from pH 7 to pH 12. The relation between Zeta potential and pH for silica sample is shown in Fig. 3. This plot shows that the silica particles remained electronegative throughout the pH range tested and that the number of hydroxyl groups existing on the silica surface was highest when pH was 9.

2. Surface Modification

The optimal condition to modify the silica surface was proposed to be 65 °C with the surfactant-to-silica mixing ratio of 2 wt% in

Table 2. Chemical composition of silica particles obtained in this study

Composition	SiO_2	Fe	Al	Ca	Mg	Mn	B	P
Wt%	98.8731	0.0210	0.0217	0.0009	0.0005	0.0001	N.D.	N.D.

Table 3. The silica particles surface modification conditions

Sample no.	Silica (g)	CTAB (g)	CTAB/Silica (%)	Temperature (°C)
1	1.000	0.0000	0.0	-
2	1.000	0.0203	2.0	50
3	1.000	0.0304	3.0	50
4	1.000	0.0201	2.0	60
5	1.000	0.0300	3.0	60
6	1.000	0.0204	2.0	70
7	1.000	0.0301	3.0	70

the preliminary experiment. In addition, the CTAB-modified silica exerted the best properties. Therefore, silica particles were modified in this study as follows: 100 ml deionized water, 1 g silica particles, and CTAB were mixed in a flask under constant stirring, with the pH fixed at 9. The amount of CTAB was controlled at 2 or 3 wt% of that of silica. The temperature was changed from 50 °C to 70 °C. The surface modification conditions are summarized in Table 3.

Particle size distribution was measured before and after the surface modification by using the particle size analyzer, which measures particle size by using light scattering, assuming that the particles are spherical. Therefore, the particle size measured by this instrument may contain significant error if the particles are not spherical. Nevertheless, the change in particle size distribution could be observed clearly with this instrument to evaluate the effect of surface modification.

The particle size distribution of silica particles produced at different surface modification conditions is compared in Fig. 4. It is demonstrated that the size distribution of silica particles changed after the surface modification process depending on the process condition. The average size of unmodified silica particles was 240.38 nm (Fig. 4). When the silica particles were modified at 50 °C, the size distribution did not change much: the average size of sample 2 and sample 3 was 220.39 and 253.21 nm, respectively. When the modification was carried out at 60 °C, the silica particles became much

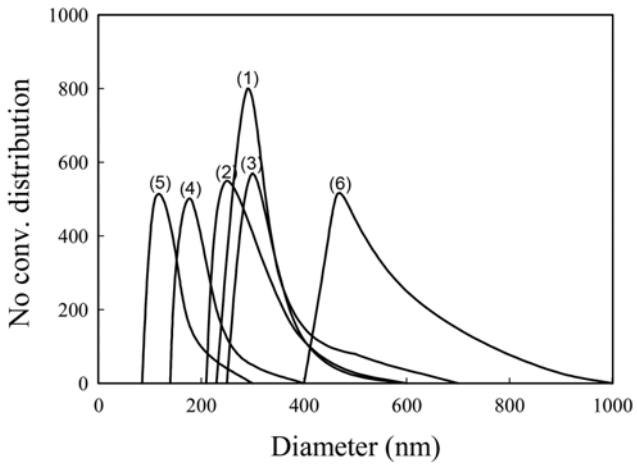

Fig. 4. Measured size distributions of silica particles before and after modification under different conditions: (1) unmodified; (2) CTAB 2%, 50 °C; (3) CTAB 3%, 50 °C; (4) CTAB 2%, 60 °C; (5) CTAB 3%, 60 °C; (6) CTAB 2%, 70 °C.

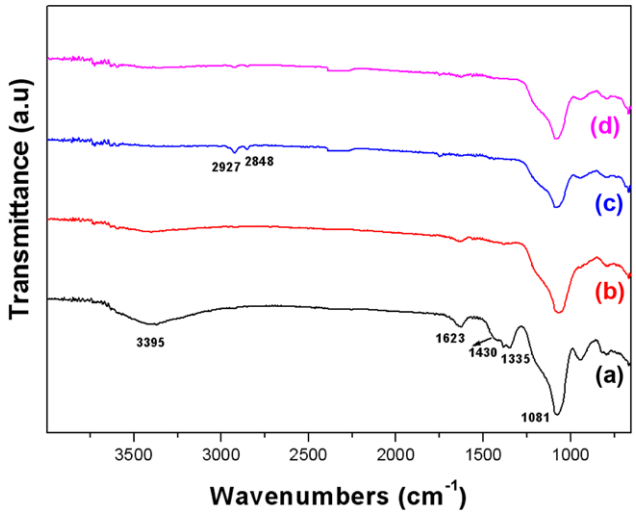

Fig. 5. FT-IR spectra of unmodified and 2 wt%-CTAB-modified silica particles: (a) unmodified; (b) modified at 70 °C, (c) modified at 60 °C, (d) modified at 50 °C.

smaller. The average size of silica particles modified with 2 wt% and 3 wt% CTAB was 145.44 and 107.89 nm, respectively, which indicates that the aggregate structure was improved as a result of the surface modification process under these conditions. When the temperature was set at 70 °C, however, the silica particles became larger: the average particle size increased to 407.54 nm. This result can be interpreted as follows: high temperature led to faster coagulation among silica particles while most CTAB were dissolved in water to form more CTAB micelles, leaving little CTAB available for being grafted on silica particle surface. The SEM images of silica particles 3 wt%-CTAB-modified at 60 °C are shown in Fig. 2(c) and 2(d). Nano-sized (50-150 nm) particles with less aggregated structure are clearly shown in these figures.

The FT-IR spectra of silica particles before and after surface modification using 2 wt% CTAB at different temperatures are shown in Fig. 5. The stretching vibration of Si-O was found at 1,081 cm^{-1} in all the plots, whereas the characteristic peak of Si-O-Si at 920 cm^{-1} became weak after the surface modification process. For unmodified silica, some stretching vibration peaks were found in the spectrum. Actually, these peaks are not the characteristic peaks of silica particles. It is speculated that the peaks might stem from the material used for preparing the silica particles. Actually, the characteristic peak at 1430cm^{-1} came from the stretching vibration of Ca-O. These peaks disappeared after the surface modification process, which indicates that CTAB grafted on the surface of silica prevented the absorption of these peaks. On the curves (c) and (d) of Fig. 5, the typical stretching vibration of C-H was found at 2,848 and 2,927 cm^{-1} stemming from $-CH_2$ and $-CH_3$ in CTAB, respectively. The stretching vibration of C-H did not appear clearly in the curve (b), for which the silica particles were modified at 70 °C. This result is consistent with the size distribution result shown above. From the results obtained, the optimal condition to modify silica sample seems to be 60 °C with the CTAB-to-silica mixing ratio of 3 wt%. In addition, the peak strength around 3,400 cm^{-1} corresponding to -OH on the surface of silica particles decreased after surface modification, which indicates the existence of surfactants on the surface of silica

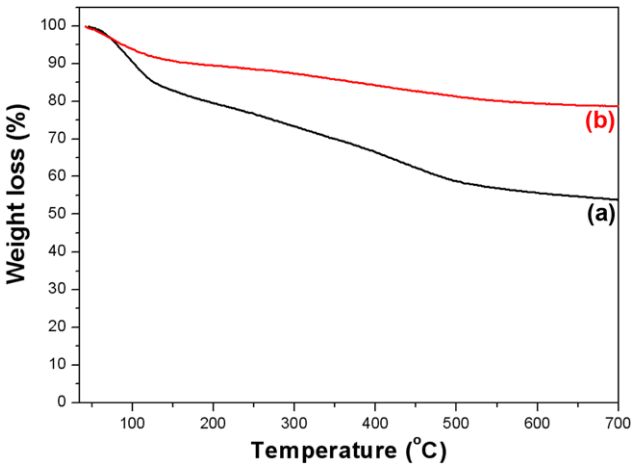

Fig. 6. TGA plots of (a) unmodified silica and (b) 2 wt% CTAB-modified silica at 60 °C.

nanoparticles.

Fig. 6 shows TGA plots of unmodified and 2 wt% CTAB-modified silica samples. The obvious weight loss of the samples could be found in the plots. At low temperature (<200 °C), the weight loss is caused by the removal of water attached on the particle surface. When the temperature increased from 200 °C to 800 °C, the weight loss was derived from the dehydration condensation of Si-OH in silica molecules. As shown in Fig. 6, the weight loss of CTAB-modified silica was smaller than that of unmodified silica, which indicates that the CTAB-modified silica made less water absorption on silica surface. In particular, the weight loss of unmodified silica sample from 200 °C to 500 °C was larger than that of the CTAB-modified silica, which suggests the possibility of the existence of some other organic substances on the unmodified silica. This result is consistent with the unusual stretching vibration peaks found in the FT-IR spectrum.

3. Recovery of Calcium Nitrate

After the reaction of slag and nitric acid and filtration of insoluble silica, the remaining solution contains not only excess nitric acid and calcium nitrate but also tiny amount of nitrates of metals originating from slag as is shown in the following.

$$FeO+2HNO_3 \rightarrow Fe(NO_3)_2+H_2O \quad (2)$$

$$Al_2O_3+6HNO_3 \rightarrow 2Al(NO_3)_3+3H_2O \quad (3)$$

$$MgO+2HNO_3 \rightarrow Mg(NO_3)_2+H_2O \quad (4)$$

In this study, the calcium nitrate yield was enhanced by adding CaO into the solution to neutralize excess nitric acid. During this process that increases pH of the solution considerably, some metal components were replaced by calcium due to the hydroxide precipitates having lower solubility products as is shown in the following. The solubility product constants of metal hydroxides are shown in Table 4.

$$Fe(NO_3)_2(aq)+CaO+H_2O \rightarrow Ca(NO_3)_2(aq)+Fe(OH)_2 \downarrow \quad (5)$$

$$2Al(NO_3)_3(aq)+3CaO+3H_2O \rightarrow 3Ca(NO_3)_2(aq)+2Al(OH)_3 \downarrow \quad (6)$$

$$Mg(NO_3)_2(aq)+CaO+H_2O \rightarrow Ca(NO_3)_2(aq)+Mg(OH)_2 \downarrow \quad (7)$$

Table 4. Solubility product constants of metal hydroxides

alt	Solubility equilibrium	Ksp
$CaCO_3$	$CaCO_3(s) \leftrightarrow Ca^{2+}(aq)+CO_3^{2-}(aq)$	9×10^{-9}
$Ca(OH)_2$	$Ca(OH)_2(s) \leftrightarrow Ca^{2+}(aq)+2OH^-(aq)$	6.5×10^{-6}
$Mg(OH)_2$	$Mg(OH)_2(s) \leftrightarrow Mg^{2+}(aq)+2OH^-(aq)$	7.1×10^{-12}
$Fe(OH)_2$	$Fe(OH)_2(s) \leftrightarrow Fe^{2+}(aq)+2OH^-(aq)$	2×10^{-15}
$Fe(OH)_3$	$Fe(OH)_3(s) \leftrightarrow Fe^{3+}(aq)+3OH^-(aq)$	1.1×10^{-36}
$Al(OH)_3$	$Al(OH)_3(s) \leftrightarrow Al^{3+}(aq)+3OH^-(aq)$	2×10^{-33}

After other metal components were removed as hydroxide precipitates, calcium nitrate was obtained in a crystallizer wrapped with a cooling water jacket. The volume of the crystallizer was about 2 L. During the calcium nitrate enrichment process, the solution was heated. Then the warm concentrated calcium nitrate solution was put into the crystallizer; it was stirred uniformly while the crystallizer wall was cooled down using cooling water provided from a circulating chiller. Under this condition, calcium nitrate began to crystallize at about 35 °C. It was found that the enriched solution had a high specific gravity (1.63-1.65), which is equivalent to the concentration of 85-90%; it is preferable to obtain calcium nitrate efficiently. The purity of the extracted calcium nitrate was more than 99.99%.

CONCLUSION

High purity nano silica was synthesized by using acid treatment and surface modification from blast-furnace slag generated in the steel industry. The conclusions obtained from the experimental results are as follows:

(1) Blast slag was treated with nitric acid to extract high-purity insoluble silica particles. The diameters of extracted silica particles were about 30-50 nm observed by FE-SEM and the size distribution of silica nano-particles was 240.38 nm characterized by particle size analyzer.

(2) Then, high purity silica nano-particles were obtained by filtration and were surface modified by CTAB. Synthesized silica remained electronegative throughout the pH range tested, and the number of hydroxyl groups existing on the silica surface was highest when the pH was 9.

(3) The size distribution of silica particles was smallest when the modification temperature was 60 °C. The average size of silica particles modified with 2 wt% and 3 wt% CTAB was 145.44 and 107.89 nm, respectively, while the average size of unmodified silica was 240.38 nm.

(4) On the other hand, pH of the remaining solution was adjusted by adding CaO and then high-purity calcium nitrate crystals were extracted using solubility difference. It was found that the enriched solution had a high specific gravity (1.63-1.65), which is preferable for obtaining calcium nitrate efficiently.

REFERENCES

1. Y. Sakamotoa, Y. Tonookab and Y. Yanagisawa, *Energy Convers. Manage.*, **40**, 1129 (1999).
2. J. Maa, D. G. Evansb, R. J. Fullera and D. F. Stewart, *Int. J. Produc-*

tion Economics, **76**, 293 (2002).
3. N. Lazaric, P. Mangolte and M. Massué, *Research Policy*, **32**, 1829 (2003).
4. J. Péra, J. Ambroise and M. Chabannet, *Cement and Concrete Research*, **29**, 171 (1999).
5. S. Kourounis, S. Tsivilis, P. E. Tsakiridis, G. D. Papadimitriou and Z. Tsibouki, *Cement and Concrete Research*, **37**, 815 (2007).
6. S. Kumar, R. Kumar, A. Bandopadhyay, T. C. Alex, B. R. Kumar, S. K. Das and S. P. Mehrotra, *Cement & Concrete Composites*, **30**, 679 (2008).
7. A. Bougara, C. Lynsdale and K. Ezziane, *Construction and Building Materials*, **23**, 542 (2009).
8. J. H. Johnston, A. J. McFarlane, T. Borrmann and J. Moraes, *Current Appl. Phys.*, **4**, 411 (2004).
9. K. N. Pham, D. Fullston and K. Sagoe-Crentsil, *J. Colloid Interf. Sci.*, **315**, 123 (2007).
10. B. J. Hwang, S. W. Park, D. W. Park, K. J. Oh and S. S. Kim, *Korean J. Chem. Eng.*, **26**, 775 (2009).